1987ApJ...317..676O

THE ASTROPHYSICAL JOURNAL, 317:676–685, 1987 June 15
© 1987. The American Astronomical Society. All rights reserved. Printed in U.S.A.

FINE-SCALE MOTION IN NGC 6514 and NGC 6523

C. R. O'DELL, L. K. TOWNSLEY, AND HECTOR O. CASTAÑEDA[1]
Rice University
Received 1986 September 5; accepted 1986 December 9

ABSTRACT

Velocity maps of the inner regions of the bright H II regions NGC 6514 and NGC 6523 were made with unprecedented spatial and spectral resolution in the 5007 Å line of [O III]. In addition to the advantages of an instrumental full width at half-maximum intensity of only 5.4 km s^{-1}, the small thermal width of the heavy oxygen ion also allows determination of accurate line widths and velocities. The CCD spectra were numerically fitted to Gaussian line profiles and revealed two separate velocity systems in NGC 6523. The data sets of radial velocities were used to derive the dependence of the most probable turbulent velocities upon the sample sizes, and the spatial dependence of the structure function. These relationships are the basic functions for comparison with the predictions of the models for turbulence in H II regions.

Subject headings: nebulae: H II regions — nebulae: individual (NGC 6514, NGC 6523) — turbulence

I. INTRODUCTION

The last decade has seen a significant growth in the number and quality of studies of the motion in Galactic H II regions. This growth has been accompanied by a parallel improvement in theory, so that we now realize that the dynamical behavior of H II regions is much more complex than was originally envisioned. The early picture of Strömgren of spherical nebulae in the middle of an un-ionized cloud has given way to a recognition that a strong observational effect operates, so that many of the optically bright H II regions are objects formed near the surface of larger neutral clouds. At the same time Spitzer's model of a slowly expanding enclosed nebula, driven by gas pressure differences, has been supplemented by models recognizing the importance of stellar winds and the enormous pressure differences that can occur when the ionization boundary reaches the edge of the neutral cloud. In a series of papers, the senior author and his colleagues have published observational maps of the velocities of a number of H II regions (NGC 2237–2246, Fountain, Gary, and O'Dell 1979; NGC 6611, Mufson *et al.* 1981; NGC 1499, NGC 7000, and IC 1318B/C, Fountain, Gary, and O'Dell 1983*a*; S252, Fountain, Gary, and O'Dell 1983*b*) which reveal evidence for all of the major theoretical driving mechanisms.

The fact that H II regions should also be characterized by a superposed random motion owing to turbulence has also been recognized for some time; however, there have not been many observational attempts to test the existing rudimentary theory. The subject merits investigation because we know that transfer of kinetic energy through turbulent elements of successively smaller sizes must transfer energy from the large-scale motion of the nebula down to elements small enough in size that the Reynolds number is small and the energy is deposited through viscosity. The magnitude of this mechanism and its impact on processes such as star formation remain unknown.

There have been some observational investigations that have attempted to provide data for testing of turbulence theory. An early detailed mapping of radial velocities in the Orion Nebula (NGC 1976, M42) by Wilson *et al.* (1959) was used by Münch (1958) to test existing theory. However, the Ph.D. thesis work of Castañeda (1985) has shown that even the central regions of the Orion Nebula are characterized by multiple velocity systems, only partially recognized by Wilson *et al.* (1959) which confuse any interpretation. Scalo (1984) has attempted to use radio observations of CO in the ρ Ophiucus cloud to perform a statistical analysis of turbulent motion, although at low spatial resolution. The most ambitious attempts to characterize fine-scale motions in H II regions have been the studies of Jean René Roy and his colleagues of M17 (Roy, Arsenault, and Joncas 1986) and S142 (Roy and Joncas 1985). In this case the Fabry-Perot technique was used at a good velocity resolution (20 km s^{-1}) and velocity accuracy (2–3 km s^{-1}) and at nearly the seeing limit of angular resolution. A contrasting but equally useful study was that of O'Dell (1986), who used data obtained in mapping the large-scale motion of H II regions to determine the statistical nature of the random motions.

The potential exists to provide much better observational data. Stigmatic spectrographs of high through-put now exist, as do two-dimensional CCD (charge-coupled device) detectors, which when used in combination, can provide unambiguous information about the velocity of gas at velocity resolutions small compared with the thermal widths of the lines and at the seeing limit determined by Earth's atmosphere. This paper reports the results of an observing program intended to provide data of unprecedented accuracy. Section II describes the observations, § III, the unique method of data reduction, and § IV, the analysis of these data.

II. THE OBSERVATIONS

In order to provide data adequate to the problem at hand and to improve significantly upon the earlier work cited above, several basic considerations had to be observed. The emission line selected had to be adequate, that is, it must be characteristic of the H II region, intrinsically strong and intrinsically narrow. For this reason we chose the 5007 Å line of [O III], which is inherently strong in H II regions and has a thermal width only one-fourth that of Hα, which was the line of choice in most of the earlier studies. The angular resolution had to be adequate to allow determination of radial velocities at many

[1] Visiting Observer, Kitt Peak National Observatory, National Optical Observatories, which is operated by the Association of Universities for Research in Astronomy, Inc., under contract with the National Science Foundation.

© American Astronomical Society • Provided by the NASA Astrophysics Data System

1987ApJ...317..676O

points across the H II regions and study of the smallest possible elements. We thus chose a system that easily allowed resolution at the seeing limit of Earth's atmosphere. The spectral resolution had to be sufficiently high to allow detection of multiple-velocity components, so we used a system that would clearly resolve the emission-line thermal profile. The detector had to have a large dynamic range and possess intrinsic high quantum efficiency; therefore, we used a CCD detector. The system should be stigmatic, so that one would know exactly where it was pointed and could produce radial velocities free of the illumination effects that sometimes plague Fabry-Perot systems. We selected a grating spectrograph. Finally, one needs a data reduction system that can accurately determine radial velocities, line widths, and identify multiple components where necessary. Fortunately Rice University has one of the most powerful of such systems.

The observing system used was the coudé feed and coudé spectrograph at the Kitt Peak National Observatory. The coudé feed system is a 0.9 m aperture fixed mirror system that is fed different parts of the sky by a 1.5 m altitude-azimuth mounted flat mirror. The scale of the image at the entrance slit was $7''.2\ mm^{-1}$. Since the image field rotates as the telescope points to different parts of the sky, correction by an optical field rotator was necessary. Unfortunately, the field rotator had been designed for use with the coudé beam of the equatorially mounted 2.1 m telescope and did not provide a correct rate of field rotation correction. The correct field rotation settings were calculated throughout the exposures and set in by hand, giving position angles accurate to about 1°. The coudé spectrograph was used in its highest resolution mode for this wavelength range, giving a reciprocal dispersion of 1.1 Å mm^{-1}. The entrance slit of 0.18 × 25 mm was projected on to the RCA-CCD No. 2. The method of calibrating the angular scale on the detector has been described before (O'Dell and Ball 1985) and was $0''.406\ pixel^{-1}$. The velocity scale was determined from the wavelengths of thorium and argon comparison lines straddling the 5007 Å line and was 1.738 km s^{-1} per pixel. Traces of the profiles of the comparison lines show that the characteristic full width at half-maximum intensity (FWHM) was 5.36 ± 0.26 km s^{-1}. The only important disadvantages of this observing system were the extra reflections inherent in the coudé system and the inability to use a multiple-entrance slit, as was done by Wilson *et al.* (1959) for their study of the Orion Nebula.

The nebulae observed were NGC 6514 (M20, the Trifid nebula) and NGC 6523 (M8, the Lagoon nebula). Both satisfied the basic constraints for inclusion in this program; that is, they are intrinsically bright, they possess circular symmetry, have been observed by other methods, and have guide stars bright enough to appear on the high-resolution spectra as fiducial marks. The guide stars used were SAO 186145 for NGC 6514 and SAO 186204 (9 Sgr) for NGC 6523. In the case of NGC 6514 the slits were close to the center of symmetry of the nebula (cf. Lynds, Canzian, and O'Neil 1985) while the guide star for NGC 6523 was well removed from the complex Hourglass region (Lynds and O'Neil 1982; Woodward *et al.* 1986). The 2′ long slit covered only the innermost sections of both nebulae and represent a sample of only a few percent of the total frontal area.

The method of adjustment of the focus of the spectrograph was to vary the position of the detector until the FWHM of the comparison lines had reached a minimum. Photometric calibrations of the field were made by quartz continuum lamp exposures. The wavelength calibration was determined by comparison spectrum exposures made before and after each nebular exposure, this frequent a determination being necessary due to the detector shifting slightly as the liquid nitrogen coolant boiled off during the night.

The exposures were made by placing the guide star as near to the center of the entrance slit as possible. This was very accurately done across the slit, but spectra obtained on different nights and observing runs would often have the stellar continuum spectrum located at different positions. The position angle was always specified beforehand and the appropriate adjustments made to the image rotator during an exposure.

The exposures used in our reduction and analysis are shown in Table 1, which gives the date of observation, position angle, and exposure time. When the sky conditions were clear, an exposure of 2 hr would give a peak signal-to-noise ratio per pixel of 8.2 for NGC 6514 and an exposure of 1.5 hr would give 21.9 for NGC 6523.

III. DATA REDUCTION

The raw material of the data reduction was the series of exposures of the nebulae, the comparison lamp, and the continuum lamp. The final product is a set of radial velocities, FWHM values, and intensities for all velocity systems covered by an exposure. The data reduction on the mountain was straightforward, being the subtraction of bias signals, followed by point-to-point sensitivity determination and application of the corresponding flat-field correction. At Rice we first divided the two-dimensional spectra into a series of one-dimensional spectra by averaging over intervals of five rows, corresponding to about the seeing limit of 2″. The zero point for these individual spectra was set at the guide star, and this was determined

TABLE 1

RECORD OF OBSERVATIONS

Date	Position Angle	Exposure Time (hr)
	NGC 6514	
1984 May 22	180°	1.0
	90	2.0
1984 May 23	180	2.0
	45	2.0
1984 May 24	135	2.0
1984 May 25	210	2.3
1985 Apr 29	163	2.0
1985 Apr 30	270	2.0
	225	2.0
1985 Jul 2	210	2.0
1985 Jul 4	315	2.0
1985 Jul 9	270	2.0
	NGC 6523	
1984 May 22	90	1.0
1984 May 23	180	1.1
1984 May 24	135	1.5
	225	1.5
1984 May 25	210	1.5
1985 May 1	270	2.0
1985 May 2	180	1.5
	225	1.5
	315	1.5
1985 Jul 5	210	1.5
	270	1.4
1985 Jul 6	300	1.5
1985 Jul 8	300	1.4

© American Astronomical Society • Provided by the NASA Astrophysics Data System

1987ApJ...317..676O

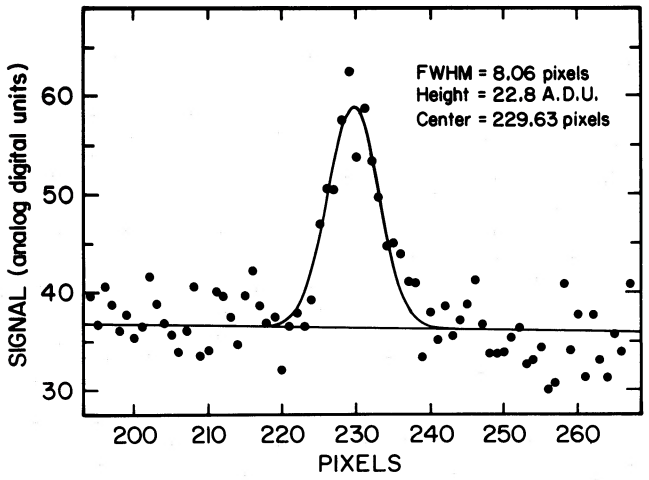

FIG. 1.—A characteristic spectrum for NGC 6514, including values for the FWHM of the Gaussian curve fit to the data.

by measuring the intensity of the stellar continuum spectrum perpendicular to the wavelength dispersion. By this means we had a common reference point for spectra obtained on different nights. Because the guide star was not always at the same slit position along the slit, some spectra near the ends of the slit do not have as much redundancy as those near the middle.

The individual spectra were reduced using the Rice University Picture Processing Facility, a computer system developed (Jensen, Talbot, and Dufour 1981) for analyzing two-dimensional images. We employed a special line-fitting program developed by J. J. Hester. This program determines the best fitting Gaussian line profiles under assumptions of number, approximate location, and width of line components determined by the operator. The quality of the fit was determined by simultaneously-derived χ^2 functions. The result of these fitting studies were peak intensities, integrated areas, FWHM (corrected for the predetermined instrumental broadening), and radial velocities of each line component. There were two distinct velocity components in NGC 6523, but only one could be discerned in the noisier NGC 6514 data. In the central region of NGC 6523 the difference in radial velocities of the two systems was such that higher peak intensity component NGC 6523A had a more positive value than the weaker component (NGC 6523B). Component A was narrower (FWHM $= 8.5 \pm 0.1$ km s^{-1}) than component B (FWHM $= 11.7 \pm 0.3$ km s^{-1}), and the ratio of peak intensities was 4.6 ± 0.5. Characteristic results for the central region of each nebula are shown in Figures 1 and 2. The wavelength calibration was determined from the comparison lamp exposures, where we allowed for tilt and distortion of the two-dimensional spectra, in addition to the slow drift in position. The radial velocities were then corrected to heliocentric velocities which can be converted to local standard of rest velocities by adding 11.7 km s^{-1} (Elliot *et al.* 1984). The averaged results are shown in Tables 2, 3, and 4.

The accuracy of these results can be measured by the dispersion of values for spectra covering the same part of the nebulae. This dispersion was calculated by looking at values for the central five spectra at all position angles. For the more intense system NGC 6523A, the dispersion of velocities was 0.53 km s^{-1}. For the less intense system NGC 6523B the dispersion was 1.30 km s^{-1}. In the single-velocity system for NGC 6514 the dispersions for radial velocity was 1.24 km s^{-1}. The central heliocentric values for NGC 6514, NGC 6523A, and NGC 6523B were -0.11 ± 0.55, -3.23 ± 0.22, and -7.95 ± 0.53 km s^{-1}, respectively.

IV. DATA ANALYSIS

The goal of our data analysis was to derive statistical functions that could be compared with the predictions of current theories and could guide in the development of more refined theories of turbulence. The specific tasks were to derive dispersions and structure functions for both nebulae.

Since what we seek is a statistical analysis of the random motions, we must first remove any large-scale motions that arise from systematic gas flow. Examination of the data showed that there was a general circular symmetry of the radial velocities about the values at the guide stars. In NGC 6514 this symmetry was well defined for all position angles except 90°, and we applied a correction of $\Delta V = -0.0392|\phi|$ km s^{-1} per pixel, where ϕ is the displacement from the guide star. This means that for the spectrum centered at 10 pixels above the center of the slit, a correction of 0.39 km s^{-1} was applied. For position angle 90° no correction was necessary for

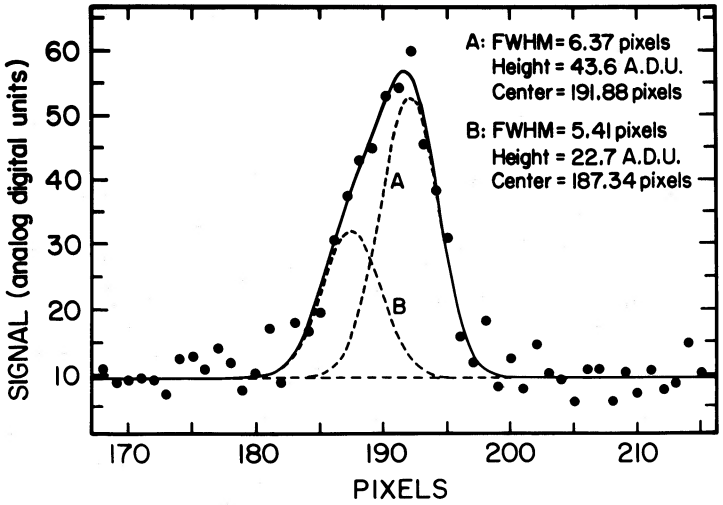

FIG. 2.—The same as Fig. 1 except for NGC 6523. The FWHM and intensity is shown for both components of the observed line.

© American Astronomical Society • Provided by the NASA Astrophysics Data System

1987ApJ...317..676O

TABLE 2

HELIOCENTRIC VELOCITY AND FWHM DATA FOR NGC 6514[a]

θ	Position Angle					
(")	45°	90°	135°	163°	180°	210°
71.0	4.83/ 9.62	-0.08/12.83			5.16/15.45	8.87/ 9.02
69.0	6.10/ 5.78	0.22/19.68	6.22/12.26		5.34/ 5.60	7.42/ 4.89
67.0	4.39/13.54	-1.39/18.14	2.59/ 8.14	3.53/12.60	7.11/10.01	8.83/ 6.61
65.0	6.81/19.80	1.76/21.06	5.47/13.13	2.84/14.40	6.80/11.46	
62.9	5.07/15.21	0.14/12.41	3.68/13.49	1.99/10.70	7.60/ 9.64	
60.9		-0.09/20.06	2.93/15.44	2.73/14.24	6.23/ 9.90	
58.9		0.42/15.27	2.67/17.01	2.99/11.95	6.19/10.88	
56.8	3.56/16.46	-0.56/17.34	-0.12/15.52	1.82/16.53	5.72/ 9.29	
54.8		-0.22/28.85	3.30/17.47	3.91/17.64	7.35/ 7.07	
52.8	7.25/ 7.48	-2.35/19.05	2.33/17.77	0.52/14.27	6.49/10.38	
50.8		-3.36/22.20	1.15/16.23	0.96/13.01	7.03/10.40	
48.7		2.10/20.97	3.08/16.38	0.08/15.01	6.07/ 9.36	
46.7		-0.22/16.78	0.02/16.13	1.03/21.01	6.37/11.50	
44.7		-2.66/20.65	3.02/14.77	1.82/28.06	5.52/14.69	
42.6		0.86/17.78	2.51/19.59	2.24/14.64	7.45/ 7.32	
40.6		0.10/19.17	-0.26/12.17	1.53/19.77	5.37/11.82	
38.6		-2.08/16.94	0.87/16.02	-1.87/15.07	4.60/15.16	
36.5		-0.42/16.93	-0.99/22.22	3.65/17.17	5.35/10.44	
34.5		-0.51/23.03	1.62/19.32	9.90/18.80	6.78/ 9.36	
32.5	1.25/22.36	-0.84/23.57	0.71/18.06	-1.61/12.57	6.78/ 7.07	
30.4	-1.86/20.40	-1.10/24.26	-0.43/16.66	1.00/24.40	3.71/ 9.01	6.17/ 7.88
28.4	0.29/15.17	-1.44/21.09	-0.85/16.29	1.37/13.91	4.09/15.74	5.59/18.87
26.4	-1.33/20.68	0.90/21.32	-1.44/21.39	-2.83/ 9.88	3.04/11.05	6.77/13.41
24.4	-0.88/17.67	-3.47/18.64	-1.37/18.21	-3.71/16.83	2.50/ 9.79	7.43/13.72
22.3	-2.75/21.02	-0.66/24.05	-5.77/22.55	-2.73/ 9.16	3.50/12.34	5.71/12.29
20.3	-0.94/20.09	-2.42/24.49	-2.97/15.83	-4.00/10.21	2.39/12.18	3.61/15.99
18.3	-0.97/22.17	-2.83/23.98	-1.44/17.16	-3.32/15.74	2.01/ 9.01	3.36/14.52
16.2	-0.75/21.36	-2.91/20.92	-2.81/17.22	-0.67/15.45	2.86/ 9.64	1.46/13.03
14.2	-1.75/18.83	-1.70/18.58	-2.04/16.16	-5.08/ 9.45	1.44/12.36	2.61/12.47
12.2	-3.57/13.12	-1.28/22.51	1.92/20.97	-2.74/22.66	1.04/11.69	1.68/12.16
10.2	-4.22/20.77	-2.57/22.49	0.02/19.56	-3.28/15.05	2.35/17.92	2.78/12.27
8.1	-5.82/12.32	-0.02/21.67	-2.37/14.86	-1.08/21.67	1.84/12.57	1.91/12.10
6.1	-1.51/24.08	-2.42/15.45	-2.84/15.44	-1.35/24.81	3.16/10.73	1.71/12.75
4.1	-0.39/20.05	-1.01/18.15	-1.39/21.52	-1.40/20.72	1.34/13.31	1.10/17.58
2.0	-0.23/16.14	-2.10/13.38	0.67/18.22	-0.87/18.24	0.29/13.87	2.13/15.18
0.0	-2.16/ 9.57	-1.29/16.20	1.29/21.09	0.39/20.38	1.65/11.53	-0.56/13.52
-2.0	-1.72/18.31	-1.20/16.23	-0.47/13.41	-1.42/14.17	1.17/10.13	0.91/20.43
-4.1	-0.99/ 8.67	-1.59/13.72	-0.50/13.30	-3.57/17.94	-0.14/16.21	-0.30/14.79
-6.1	-0.91/23.13	-1.82/13.12	0.03/12.84	-2.92/14.23	-1.97/14.03	-0.99/20.33
-8.1	0.05/16.63	-2.00/11.80	-0.64/14.79	-4.69/14.67	0.06/10.20	-1.53/16.67
-10.2	0.32/20.81	0.53/14.93	1.68/14.27	-5.36/ 8.39	0.33/13.23	-0.32/17.30
-12.2	0.55/17.56	-0.09/16.14	1.00/13.97	-5.98/ 7.88	-0.56/16.21	1.04/18.91
-14.2	2.22/16.60	1.13/17.69	0.11/16.53	-3.07/18.90	-0.20/15.29	-1.41/14.68
-16.2	1.23/13.13	0.56/12.52	0.76/15.84	-3.27/11.80	-1.00/15.39	-1.59/16.32
-18.3	4.67/13.11	-1.91/26.18	1.93/11.89	-1.95/17.96	-0.58/12.77	0.08/20.78
-20.3	-1.13/25.07		3.71/12.03	-3.87/ 8.33	0.60/13.68	1.01/17.80
-22.3	2.40/11.77		2.65/12.62	-3.36/13.24	0.80/16.78	1.50/20.43
-24.4	2.40/ 7.70			-0.50/14.25	1.84/18.94	3.96/22.04
-26.4	-2.95/13.76				3.18/14.83	4.17/13.81
-28.4	4.96/13.88				-4.61/13.18	5.17/18.36
-30.4	0.02/10.94					
-52.8			3.37/10.00			
-54.8			5.52/ 2.33			
-56.8			3.90/16.23			
-58.8			1.37/15.26			
-60.9			1.63/19.96			
-62.9			4.42/10.19			

[a] First entry is heliocentric velocity; second entry is FWHM, both in km s^{-1}.

© American Astronomical Society • Provided by the NASA Astrophysics Data System

1987ApJ...317..676O

TABLE 3

HELIOCENTRIC VELOCITY AND FWHM DATA FOR NGC 6523A[a]

θ	Position Angle						
(")	90°	135°	180°	210°	225°	240°	300°
75.1					-5.36/ 7.21		
73.1				-6.68/ 8.47	-5.37/ 7.18		
71.0			-8.34/10.00	-7.53/ 7.46	-5.69/ 8.22		
69.0	-5.49/ 5.02	-7.27/ 7.33	-8.34/10.15	-6.70/ 8.39	-5.47/ 8.60		
67.0	-5.23/ 6.18	-7.48/ 5.09	-7.62/ 7.70	-6.96/ 8.72	-5.68/ 8.16	-9.74/10.64	-6.51/11.81
65.0	-5.16/ 4.78	-7.52/ 6.04	-7.75/ 9.46	-13.50/ 8.30	-5.74/12.33		-5.17/10.58
62.9	-4.77/ 6.33	-7.79/ 6.72	-6.94/10.06	-5.47/ 6.78	-4.41/10.41		-4.60/ 7.39
60.9	-4.79/ 7.03	-8.18/ 6.09	-8.13/10.65	-4.97/ 7.44	-2.37/10.21		-6.59/11.36
58.9	-4.78/ 6.01	-8.72/ 5.90	-4.87/ 3.72	-5.62/ 7.92	-2.31/ 8.67	-21.49/ 3.41	-5.08/ 8.75
56.8	-4.80/ 6.50	-6.11/ 9.60	-5.01/ 4.16	-4.77/ 7.65	-2.07/ 6.60	-3.79/ 4.74	-4.46/ 9.37
54.8	-4.87/ 7.41	-8.42/ 7.25	-4.93/ 3.70	-3.85/ 5.60	-2.13/ 6.20	-5.18/10.87	-5.11/ 8.89
52.8	-4.76/ 6.98	-7.35/ 8.48	-5.64/ 4.77	-3.68/ 5.78	-1.20/ 7.98	-3.62/ 7.50	-5.21/ 8.61
50.8	-5.20/ 7.13	-6.94/ 7.25	-5.15/ 6.09	-4.06/ 7.38	-1.68/ 6.63	-2.51/ 6.17	-5.91/11.58
48.7	-5.12/ 6.17	-8.76/ 7.21	-4.26/ 4.38	-3.83/ 5.11	-2.20/ 9.02	-5.33/11.58	-5.80/ 8.76
46.7	-4.95/ 6.17	-6.35/ 7.21	-4.07/ 5.25	-2.73/ 4.63	-1.49/ 6.94	-3.96/10.15	-6.03/11.03
44.7	-4.74/ 6.14	-6.34/ 7.38	-3.71/ 4.16	-2.64/ 4.61	-2.02/ 9.31	-4.26/ 9.84	-4.98/ 6.05
42.6	-5.00/ 6.73	-6.29/ 8.19	-5.36/ 9.08	-2.37/ 4.63	-1.46/ 8.46	-4.44/10.27	-3.70/ 6.47
40.6	-5.07/ 7.68	-6.45/ 8.33	-4.00/ 7.53	-2.85/ 5.86	-2.17/10.44	-5.13/11.72	-5.56/11.02
38.6	-4.86/ 7.38	-5.99/ 8.94	-3.55/ 7.03	-2.20/ 4.66	-1.43/ 7.29	-3.61/ 7.37	-5.61/11.40
36.5	-4.95/ 7.83	-5.62/ 7.82	-3.64/ 8.53	-2.68/ 6.33	-1.03/ 7.52	-3.40/ 6.29	-5.44/11.53
34.5	-4.53/ 7.58	-5.58/ 8.14	-2.77/ 8.57	-3.40/ 9.21	-0.51/ 7.23		-3.01/ 7.82
32.5	-4.97/ 8.08	-4.78/ 7.71	-3.45/ 7.27	-2.42/ 6.61	-0.39/ 7.55	-3.72/ 7.13	-3.87/ 9.11
30.4	-5.42/ 8.77	-4.98/ 7.63	-4.34/10.14	-1.24/ 4.44	-0.81/ 6.54		-5.59/13.58
28.4	-5.77/ 8.67	-5.38/ 8.36	-3.67/ 8.54	-1.32/ 5.71	-0.99/ 5.48	-3.90/ 9.25	-4.33/10.18
26.4	-6.40/ 8.25	-5.02/ 8.39	-2.93/ 6.21	-1.65/ 6.42	-0.45/ 5.71	-4.48/ 9.55	-4.18/13.95
24.4	-6.59/ 8.11	-5.61/10.88	-2.51/ 6.70	-1.47/ 5.77	-0.38/ 8.35	-3.02/ 7.52	-4.80/13.04
22.3	-6.58/ 7.95	-5.42/ 9.49	-3.78/ 8.90	-1.35/ 7.02	-1.34/ 6.93	-3.04/ 7.22	-4.74/12.48
20.5	-6.56/ 8.79	-4.65/ 8.11	-2.75/ 8.83	-0.33/ 5.35	-0.79/ 4.25	-1.79/ 5.06	-4.61/ 9.63
18.3	-6.54/10.14	-5.06/11.18	-3.93/ 9.22	-1.84/ 7.01	-1.97/ 8.82	-2.92/ 4.71	-4.96/14.32
16.2	-7.15/ 8.72	-4.05/ 9.65	-4.65/11.26	-3.31/ 6.83	-0.71/ 7.42	-2.18/ 8.77	-4.43/11.04
14.2	-6.09/10.10	-4.14/10.06	-4.91/12.90	-6.06/ 5.45	-0.96/ 8.15	-2.93/ 8.59	-5.26/11.91
12.2	-6.17/11.69	-3.78/ 7.98	-3.52/ 9.17	-3.05/ 4.95	-2.36/10.38	-4.10/10.69	-3.07/ 6.69
10.2	-5.01/ 8.31	-3.68/13.36	-3.73/13.38	-2.74/ 6.54	-2.20/10.21	-3.34/ 7.10	-3.69/ 9.77
8.1	-5.35/10.10	-3.69/ 5.35	-3.62/11.47	-2.55/ 8.33	-1.83/ 9.45		4.28/11.65
6.1	-4.67/10.32	-4.22/15.05	-3.66/11.02	-2.16/ 7.33	-2.10/ 8.30		-4.35/10.29
4.1	-4.49/ 9.54	-3.68/11.46	-3.24/ 5.38	-3.27/ 7.17	-3.32/ 9.24		-3.60/12.21
2.0	-3.76/ 8.75	-2.67/ 8.06	-2.77/ 8.81	-3.11/ 8.03	-2.35/ 9.97	-4.05/ 7.16	-4.27/12.22
0.0	-2.81/ 7.16	-3.06/10.96	-2.93/ 9.45	-3.38/ 5.34	-2.98/10.53	-4.20/ 2.30	-3.87/ 7.46
-2.0	-3.45/10.41	-2.80/ 6.27	-3.36/ 9.19	-3.82/ 9.89	-3.73/ 9.55	-4.21/ 8.34	-5.27/13.23
-4.1	-3.87/ 9.27	-3.46/ 8.94	-3.84/ 8.05	-3.24/ 0.76	-3.66/10.65	-5.74/10.19	-5.67/12.35
-6.1	-4.05/10.54	-4.22/ 9.16	-4.56/12.13	-4.46/ 9.04	-3.55/ 9.90		-6.37/11.29
-8.1	-3.79/10.14	-4.09/ 9.76	-4.33/10.29	-5.25/11.56	-3.82/13.32		-5.00/11.32
-10.2	-3.37/ 9.34	-3.70/10.30	-4.80/10.65	-5.01/10.99	-3.37/ 9.23		-5.36/ 6.69
-12.2	-4.22/11.21	-3.42/ 8.00	-5.16/14.02	-3.73/ 9.19	-4.87/10.10		-6.13/ 9.45
-14.2	-4.10/ 8.65	-3.62/ 9.33	-5.05/11.21	-5.44/ 9.68	-5.07/ 7.87	-6.57/ 7.74	-6.81/10.96
-16.2	-4.03/ 7.80	-2.96/ 7.52	-5.03/10.70	-5.93/11.71	-4.96/ 8.98		-6.56/ 9.89
-18.3	-3.76/ 9.23	-3.85/10.47	-5.72/10.87	-6.20/10.99	-5.48/ 8.39		-6.40/ 9.47
-20.3	-4.13/ 9.29	-3.14/ 8.28	-6.20/11.33	-6.28/11.31	-5.65/ 7.13	-6.32/13.09	-5.47/ 7.89
-22.3	-3.63/ 9.89	-7.17/12.96	-6.48/12.67	-6.25/11.22	-5.38/ 8.37		-5.96/ 9.18
-24.4	-3.39/ 6.54	-6.75/13.54	-6.59/10.38	-6.55/10.24	-5.55/ 7.87	-4.76/ 6.06	-5.66/11.37
-26.4	-3.62/ 8.33	-3.35/ 8.66	-7.03/11.83	-7.66/ 8.02	-5.45/ 8.31		-5.78/ 8.83
-28.4	-5.42/11.70	-1.94/ 7.11	-9.83/ 7.39	-6.58/ 9.48	-4.93/ 8.14	-4.96/ 5.52	-5.37/ 9.92
-30.4	-4.22/10.46	-2.50/ 6.84	-7.57/10.39	-6.14/ 8.22	-4.87/ 5.89	-6.15/ 5.42	-4.94/10.14
-32.5	-2.79/ 6.48	-3.30/ 6.77	-7.46/ 9.80	-5.82/ 8.02	-4.26/ 6.39		-5.14/ 6.84
-34.5	-4.74/10.47	-4.23/ 5.92	-6.67/ 9.70	-5.49/ 5.89	-4.40/ 5.18	-5.09/ 5.89	-5.22/ 8.76
-36.5	-3.41/ 9.60	-4.72/ 8.08	-6.35/10.75	-5.21/ 6.69	-4.40/ 7.23		-5.55/ 8.67
-38.6	-5.88/12.79	-5.46/ 8.82	-5.91/ 9.25	-4.73/ 3.92	-4.26/ 7.06	-5.38/ 7.02	-5.48/ 8.18
-40.6	-5.61/11.36	-5.44/ 7.99	-5.30/ 6.65	-4.59/ 2.75	-4.02/ 6.66	-5.01/ 5.85	-5.72/ 7.58
-42.6	-6.15/11.01	-5.42/ 8.70	-6.15/ 7.93	-4.46/ 4.95	-3.95/ 7.87	-5.64/ 8.70	-5.85/ 7.41
-44.7	-5.92/11.42	-5.30/ 7.31	-5.80/ 8.23	-5.09/ 7.23	-4.16/ 6.68		-4.66/ 5.36
-46.7	-6.43/11.39	-4.94/ 7.63	-5.66/ 6.84	-5.14/ 6.61	-4.11/ 6.54	-4.54/ 7.02	-5.93/ 4.95
-48.7	-6.75/11.38	-4.47/ 8.44	-6.09/ 7.99	-5.42/ 7.28	-4.24/ 6.21		-6.39/ 3.96
-50.8	-7.46/11.23	-4.58/ 8.11	-5.95/ 7.41	-5.83/ 7.59	-4.27/ 6.99		-5.66/ 9.56
-52.8	-7.32/ 9.05	-5.35/ 9.41	-6.53/ 7.63	-6.11/ 8.49	-4.63/ 7.94	-3.90/ 7.75	-5.59/ 7.48
-54.8	-7.87/ 8.77	-5.51/ 8.90	-6.32/ 6.61	-5.98/ 8.05	-5.06/ 4.87		-6.50/ 7.75
-56.8	-8.92/11.23	-6.11/ 9.52	-5.99/ 8.30	-6.78/ 9.46	-5.58/ 8.66	-4.05/ 6.65	-6.07/ 7.93
-58.9	-9.06/15.84	-5.59/ 8.98	-6.39/ 8.57	-6.21/ 7.11	-5.45/ 8.59		-5.95/ 5.29
-60.9	-8.82/10.03	-5.79/ 9.70	-6.14/ 8.59	-6.34/ 6.98			-5.78/ 6.47
-62.9	-9.04/12.62	-5.13/ 9.38	-6.71/ 5.15	-6.69/ 3.34			
-65.0	-9.07/11.82	-4.76/ 8.57					
-67.0	-9.37/10.94						

[a] First entry is heliocentric velocity; second entry is FWHM, both in km s^{-1}.

© American Astronomical Society • Provided by the NASA Astrophysics Data System

1987ApJ...317..676O

TABLE 4

HELIOCENTRIC VELOCITY AND FWHM DATA FOR NGC 6523B[a]

θ	Position Angle						
(")	90°	135°	180°	210°	225°	240°	300°
73.1				-14.55/ 4.87			
71.0			-6.89/ 2.01	-7.96/14.23	-5.91/17.50		
69.0	-5.96/14.27		-6.13/ 1.25	-9.64/16.19	-5.88/20.59		
67.0	-16.25/21.35	-6.11/ 9.59	-11.14/16.34	-14.77/ 5.71	-3.81/25.61		
65.0	-8.88/12.03	-5.24/ 9.59	-8.09/ 7.86	-13.71/ 8.02	-5.36/16.57		
62.9	-9.82/ 7.21	-2.12/ 5.49	-14.02/ 4.30	-12.33/ 8.91	-7.09/17.73	-9.06/25.60	-20.13/ 1.95
60.9	-0.49/25.96	-2.99/ 5.25	-5.14/ 3.66	-11.83/10.53	-18.51/ 3.34		-15.16/ 9.70
58.9	-9.65/12.20	-4.49/ 6.43	-8.53/12.24	-11.92/ 9.25	-10.00/18.49		-11.29/ 8.29
56.8	-5.42/11.28	-8.51/ 6.34	-9.29/14.30	-12.93/ 9.42	-9.50/12.41		-6.52/10.78
54.8	-8.37/12.15	-3.40/ 5.59	-8.28/14.02	-9.63/12.30	-11.89/11.13	-8.41/14.10	-13.84/ 9.62
52.8	-5.94/14.42	-11.97/ 7.87	-9.01/14.15	-12.12/10.00	-9.31/11.65	-9.25/16.32	-10.47/24.09
50.8	-18.20/23.15		-9.64/14.44	-12.94/10.77	-9.50/14.73	-13.72/15.45	-10.67/18.78
48.7	-2.93/22.79	-10.82/15.24	-9.10/12.14	-8.25/15.66	-9.37/12.72	-10.23/15.24	-13.87/ 9.80
46.7	-7.35/22.36	-12.48/ 6.89	-9.54/11.98	-7.94/10.09	-7.34/16.85	-9.03/13.44	-16.98/ 4.19
44.7	-7.21/21.01	-12.14/ 6.99	-9.01/13.22	-9.07/ 9.04	-10.32/17.98	-14.39/12.14	
42.6		-15.19/ 7.94	-15.19/ 4.58	-7.99/14.46	-10.44/12.39	-12.36/15.24	
40.6		-16.15/10.92	-12.11/10.36	-9.26/10.94	-11.74/12.36	-11.93/15.16	
38.6	-6.90/21.96		-10.16/11.90	-8.45/10.31	-12.27/11.91	-13.58/11.97	-10.83/ 7.13
36.5		-19.46/ 9.54	-11.69/10.99	-8.34/16.12	-13.67/11.95	-12.44/23.68	-14.97/17.09
34.5	-6.03/19.40	-9.85/16.64	-9.13/13.49	-14.41/ 8.97	-6.12/19.05	-10.01/12.84	
32.5		-10.74/ 9.79	-6.46/14.60	-7.58/15.99	-8.99/15.07	-10.77/10.45	-12.62/14.41
30.4	-6.26/19.62	-7.07/13.94	-14.56/ 4.37	-6.87/12.01	-7.54/15.76	-6.69/12.73	-10.39/12.80
28.4			-12.90/ 5.60	-7.80/12.51	-7.93/14.49	-10.52/12.69	-12.89/11.48
26.4		-12.93/12.40	-7.59/10.73	-6.35/15.21	-9.39/12.54		
24.4	-1.07/28.19		-6.72/15.69	-6.10/14.40	-5.53/17.68	-14.30/ 4.38	
22.3		-5.94/14.99	-10.05/17.93	-7.53/11.08	-6.21/14.20	-16.96/ 3.10	-10.07/13.25
20.3	-8.22/23.97	-10.90/ 9.56	-7.78/15.17	-5.75/10.82	-7.60/12.47	-10.43/10.50	-9.24/13.29
18.3			-9.86/14.04	-9.08/ 9.22	-5.87/16.90	-6.85/17.82	
16.2	-2.05-17.53	-12.49/10.88		-9.33/11.18	-4.08/12.50	-7.29/11.66	-14.05/ 4.35
14.2	1.14/18.43	-5.86/17.68		-6.06/14.80	-10.85/ 7.94	-7.67/15.50	
12.2	-5.46/ 3.99	-10.41/ 9.93	-5.53/18.70	-4.70/16.14	-8.99/ 8.91	-10.79/11.34	
10.2	-10.58/14.31	-3.91/ 2.66	-2.94/ 5.52	-5.02/15.31	-7.32/12.15	-12.43/ 5.75	
8.1		-3.72/14.51	-5.82/ 9.72	-5.37/16.89	-13.41/ 4.54	-14.27/ 6.87	-11.52/ 4.99
6.1	-7.46/ 8.28	-3.90/ 2.79	-5.12/12.39	-9.84/ 9.15	-12.96/ 3.14	-6.57/15.30	-8.72/ 9.92
4.1	-4.58/ 4.12		-4.54/16.60	-4.13/21.43	-9.24/10.24		
2.0	-10.30/19.19	-7.76/10.44	-6.58/15.20	-4.75/24.79			-2.59/23.92
0.0	-7.07/20.24			-8.35/23.85			
-2.0	-10.19/24.37	-4.38/17.28	-10.97/11.69	-8.15/25.81	-2.39/ 9.45	-4.51/19.68	
-4.1	-6.47/17.96	-18.04/17.38	-4.85/18.55	-4.16/12.88		-4.81/14.76	-5.70/18.36
-6.1	-14.94/ 6.10	-14.47/ 7.13	-3.41/ 4.74	-5.17/20.37	-1.22/15.83	-6.02/18.98	
-8.1	-13.15/ 8.11	-13.90/ 6.52	-9.48/17.50		-3.27/16.93	-5.62/18.24	
-10.2	-12.70/ 7.79	-13.66/ 5.09			-8.44/12.28		
-12.2	-13.14/ 7.05	-9.52/10.73	-4.73/ 3.59	-10.62/ 7.37	-3.27/ 6.37		
-14.2		-11.13/ 7.87		-4.33/16.71	-3.97/17.32		
-16.2	-10.30/10.17	-8.71/11.90			1.88/ 8.44		
-18.3	-7.45/15.09	-14.43/ 7.27	-3.77/20.09		0.29/ 8.96	-3.24/18.13	
-20.3	-12.51/ 9.76	-10.62/ 7.87				-5.76/11.66	
-22.3	-13.43/ 6.72	-1.95/ 4.81			-3.80/22.32		
-24.4	-9.08/10.99	-1.81/ 5.59		-7.87/ 1.06		-6.10/ 4.27	-9.97/12.27
-26.4	-11.14/10.92	-11.68/ 7.82		-3.17/ 8.72	1.30/ 7.82		
-28.4	-9.11/ 6.79	-9.26/ 9.82	-3.48/ 8.22		-6.51/ 8.53	-9.70/ 9.89	
-30.4	-12.39/ 7.83	-9.70/ 8.67			-0.95/ 9.37		
-32.5	-9.77/11.80	-7.96/13.06		-14.87/ 7.10	-0.67/16.17	-6.02/20.01	
-34.5	-9.31/ 9.42	-10.61/ 7.98	-8.17/17.06	-6.16/15.74	-4.94/17.41	-0.55/ 4.22	
-36.5	-12.14/ 9.68	-12.47/ 8.42		-7.39/11.26	-7.10/12.87		-5.02/14.28
-38.6	-7.88/ 5.52	-14.85/ 5.11	-10.00/14.06	-5.66/10.11	-3.65/15.54		
-40.6	-10.37/ 6.38	-11.33/10.38	-5.49/15.19	-6.39/10.84			
-42.6	-7.05/10.44	-13.74/ 5.50	-8.71/14.58	-6.58/11.46	-5.96/16.53	-15.64/11.57	
-44.7	-13.32/12.64	-11.91/10.10	-7.08/10.24	-5.42/20.37	-4.93/17.43	-8.58/16.86	
-46.7	-8.48/ 8.68	-11.24/ 9.26	-6.21/14.86	-9.53/ 8.68	-8.62/ 1.95	-4.34/ 2.45	
-48.7	-15.08/14.00	-13.19/ 8.59	-9.07/25.26	-5.56/12.48	-2.24/16.61		-6.26/15.28
-50.8	-8.34/11.44	-13.47/ 7.29	-7.20/ 8.57	-11.02/11.22	-3.54/12.57	-12.57/16.85	-11.58/22.29
-52.8	-10.51/18.13	-15.76/ 4.44	-10.64/15.36	-7.50/21.16	-3.42/11.46		-7.17/12.36
-54.8	-9.90/20.25	-14.72/ 8.56	-7.56/17.53	-11.09/20.06	-5.09/20.02		
-56.8	-7.68/11.72	-16.39/ 3.56	-16.32/ 6.50		4.23/16.77	-13.88/ 9.25	-14.13/ 1.86
-58.9	-7.92/ 9.40	-14.53/ 7.33	-8.13/15.43	-8.89/23.98	-5.79/13.59		
-60.9	-10.41/22.12	-15.60/ 6.27	-12.59/11.83	-14.42/ 2.90		-6.69/15.93	
-62.9		-14.30/ 6.43	-3.02/25.98	-6.46/13.83			-9.74/11.92
-65.0	-21.09/ 5.78	-12.64/ 7.07					
-67.0	-20.54/ 7.80						

[a] First entry is heliocentric velocity; second entry is FWHM, both in km s^{-1}.

© American Astronomical Society • Provided by the NASA Astrophysics Data System

1987ApJ...317..676O

negative displacements, and we used $\Delta V = 0.0153$ km s^{-1} per pixel for positive displacements. The flow corrections for both the A and B components of NGC 6523 were very similar and were as follows: component A, $\Delta V = 0.0187$ km s^{-1} per pixel, and component B, $\Delta V = 0.0195$ km s^{-1} per pixel.

The flow components that we see in both nebulae never exceed 5 km s^{-1} and are probably the results of the general expansion of these H II regions. The low magnitude of the flows indicates that the nebulae are quiescent objects, where there are surrounding neutral shells, rather than open, champagne flow situations. The two-component structure of NGC 6523 may correspond to fore and aft shells of H II. The limited range of distances covered by our maps excludes the use of these data in discussing the large-scale mass motion in these nebulae.

It is necessary to address the question of possible additional velocity components besides the two seen in NGC 6523 and the one in NGC 6514. The best guide to this is the FWHM value, more particularly, how the observed FWHM compares with the minimum FWHM expected, which would be due to thermal broadening. The FWHM for thermal broadening can be derived from equation (2-243) of Lang (1980) and is FWHM $= 5.37 \times t^{1/2}$ km s^{-1} for oxygen, where t is the electron temperature in units of 10^4 K. Any additional velocity component would add quadratically to this value. Since the observed FWHM for NGC 6514 and NGC 6523A and B were 15.6 ± 0.3, 8.5 ± 0.1, and 11.7 ± 0.3 km s^{-1}, this means that all of the line widths were significantly wider than the thermal widths (since t is about unity). If the broadening is due to random velocities within the dimension of the seeing disk, then Lang's equation gives most probable turbulent velocities of 8.4, 4.0, and 6.3 km s^{-1} in the three systems. It is always possible that the two components of NGC 6523 are actually composites of multiple subcomponents, although the quality of the line profile fit argues against this. An additional higher signal-to-noise ratio spectrum of NGC 6514 does have some division into two components, which could explain the extra size of its FWHM, but even there the unresolved turbulent velocities would have to be high.

We adopt as a common distance for both NGC 6514 and NGC 6523 the value of 1600 pc derived by Buscomb (1963) from a study of the cluster NGC 6514 and verified by Lynds, Canzian, and O'Neil (1985).

The first method of data analysis was determination of the dispersion of velocities as a function of sample size. The method of determination was the same as that used before by Roy and Joncas (1985) and O'Dell (1986), except modified according to the method of observations. Normally the dispersion would be calculated from all radial velocity values within a sample of a given diameter, with this sample spot moved in nonoverlapping locations until the entire two-dimensional velocity map of the nebula was covered. In the present case, where the sample of velocities is very good near the guide stars but poor at larger distances, we have altered our technique for calculation. We took nonoverlapping samples of adjacent spectra along each slit and calculated the dispersion of each sample. This dispersion value was then converted to the one dimensional most probable turbulent velocity (W) by multiplying the dispersion by $(\frac{2}{3})^{1/2}$, the conversion factor for a random distribution of velocities (O'Dell 1986). The mean value of W for all samples of that size could then be taken and

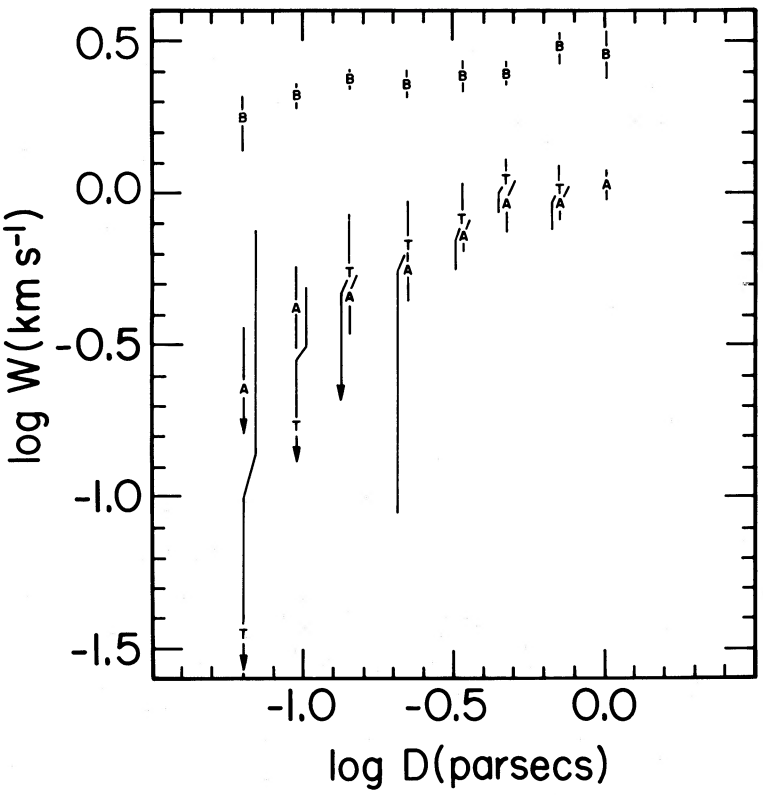

FIG. 3.—The most probable one-dimensional turbulent velocity (W) is shown for the three velocity components observed in NGC 6514 and NGC 6523 as a function of sample size. NGC 6514 is represented as the letter T, NGC 6523A as the letter A, and NGC 6523B as the letter B.

© American Astronomical Society • Provided by the NASA Astrophysics Data System

1987ApJ...317..676O

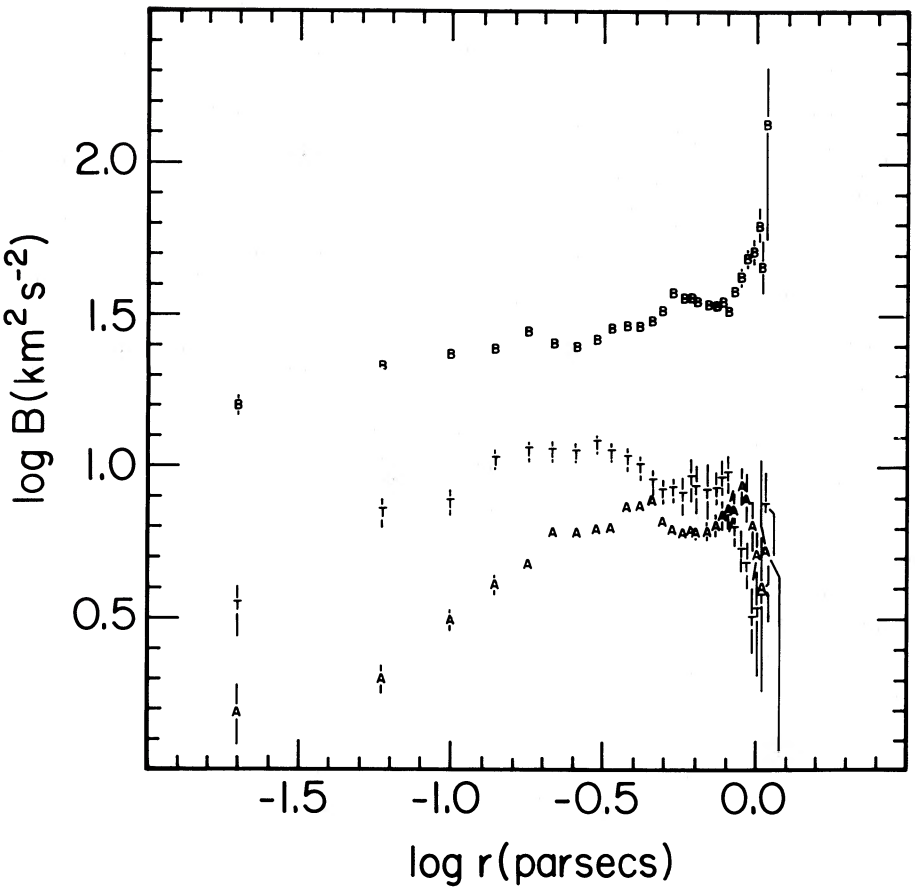

FIG. 4.—The structure function (B) is shown for the three velocity components observed in NGC 6514 and NGC 6523 as a function of the linear separation of the lines of sight. The symbols have the same meanings as in Fig. 3.

TABLE 5

MOST PROBABLE RANDOM VELOCITIES[a]

	NGC 6514			NGC 6523A			NGC 6523B		
log D	σ_{OBS}	log W	p.e. (log W)	σ_{OBS}	log W	p.e. (log W)	σ_{OBS}	log W	p.e. (log W)
−1.201.....	1.26	−1.46	$^{+1.34}_{-\infty}$	0.60	−0.65	$^{+0.21}_{-\infty}$	2.70	0.26	$^{+0.06}_{-0.13}$
−1.025.....	1.26	−0.76	$^{+0.46}_{-\infty}$	0.74	−0.37	$^{+0.14}_{-0.18}$	2.96	0.32	$^{+0.04}_{-0.05}$
−1.849.....	1.41	−0.26	$^{+0.19}_{-\infty}$	0.76	−0.35	$^{+0.08}_{-0.12}$	3.25	0.37	±0.04
−0.657.....	1.49	−0.17	$^{+0.14}_{-0.88}$	0.86	−0.26	$^{+0.08}_{-0.10}$	3.17	0.36	0.05
−0.481.....	1.60	−0.08	$^{+0.12}_{-0.17}$	1.06	−0.16	0.05	3.31	0.38	0.05
−0.326.....	1.83	+0.04	$^{+0.07}_{-0.11}$	1.24	−0.04	0.09	3.33	0.39	0.04
−0.150.....	1.76	+0.01	$^{+0.08}_{-0.13}$	1.24	−0.04	0.05	4.00	0.48	0.05
+0.003.....	...	...	...	1.40	+0.03	±0.05	3.76	0.45	±0.08

[a] All velocities are in km s^{-1} and sizes in parsecs.

© American Astronomical Society • Provided by the NASA Astrophysics Data System

1987ApJ...317..676O

the uncertainty of that mean value determined from the spread of values. This derived one-dimensional most probable turbulent velocity (W) should not be confused with the three-dimensional most probable turbulent velocity (w) computed by Roy and Joncas (1985) and Roy, Arsenault, and Joncas (1986) by multiplying the root-mean-square dispersion by $3^{1/2}$.

It is important to correct these data for the instrumental dispersion. There are random errors arising from the signal to noise of the individual spectra, right on through the data reduction procedures. The sum total of these errors is reflected in the dispersion of values derived for the same point on the nebulae. As we noted in the preceding section, the dispersion of values of the radial velocities of the three velocity systems were determined by sampling the regions very close to the guide stars and were found to be 1.24, 0.53, and 1.50 km s^{-1} for NGC 6514 and NGC 6523A/B, respectively. The true dispersion was calculated from the equation for quadratic addition used by O'Dell (1986) $\sigma^2(\text{obs}) = \sigma^2(\text{true}) + \sigma^2(\text{inst})$, where σ is the dispersion value and the parenthetical terms indicate observed, true, and instrumental values. These instrumental corrections were large for many of the smallest sample sizes where the dispersions were small. This means that the shape of the

TABLE 6

STRUCTURE FUNCTIONS[a]

	NGC 6514			NGC 6523A			NGC 6523B		
Log r	B_{OBS}	Log B	p.e. (Log B)	B_{OBS}	Log B	p.e. (Log B)	B_{OBS}	Log B	p.e. (Log B)
-1.706	4.93	0.53	$^{+0.07}_{-0.10}$	1.77	0.17	$^{+0.09}_{-0.10}$	17.92	1.20	±0.03
-1.229	8.51	0.84	$^{+0.04}_{-0.05}$	2.22	.29	±0.05	23.24	1.32	.02
-1.007	9.00	0.87	±.04	3.35	.49	.03	25.48	1.37	.02
-0.861	11.97	1.02	.03	4.30	.60	.03	26.67	1.39	.02
-0.752	12.71	1.05	.03	4.98	.67	.02	26.98	1.44	.02
-0.665	12.60	1.04	.03	6.29	.78	.02	27.54	1.40	.02
-0.592	12.51	1.04	.03	6.31	.78	.02	27.14	1.40	.02
-0.530	13.23	1.07	.03	6.42	.79	.02	28.40	1.42	.02
-0.476	12.61	1.04	.03	6.48	.79	.02	30.64	1.45	.02
-0.428	12.00	1.02	.03	7.65	.87	.02	30.92	1.46	.02
-0.384	11.29	0.99	.03	7.66	.87	.02	30.89	1.46	.02
-0.345	10.42	0.95	.03	7.52	.86	.02	32.38	1.48	.02
-0.308	9.77	0.92	.04	6.77	.81	.02	34.91	1.51	.02
- .275	9.83	0.92	.04	6.40	.79	.02	39.51	1.57	.02
- .244	9.51	0.90	.04	6.25	.78	.02	37.80	1.55	.02
- .215	10.50	0.95	.04	6.30	.78	.02	38.24	1.56	.02
- .188	9.91	0.92	.04	6.28	.78	.02	36.94	1.54	.02
- .162	9.71	0.91	.04	6.35	.78	.03	36.07	1.53	.02
- .138	9.73	0.91	.06	6.61	.80	.04	35.98	1.53	.02
- .115	10.55	0.96	.07	7.18	.84	.05	36.92	1.54	.02
-0.093	10.83	0.97	.08	7.48	.86	.06	34.16	1.50	.02
-0.073	7.71	0.79	.09	7.38	.85	.06	39.94	1.58	.02
-0.053	6.78	0.72	±0.10	8.93	.94	.06	44.13	1.62	.03
-0.034	6.27	0.68	$^{+0.13}_{-0.15}$	8.10	.89	.08	50.10	1.68	.03
-0.016	4.68	0.50	$^{+0.14}_{-0.21}$	6.63	.80	.08	53.06	1.71	.04
+0.001	4.84	0.52	$^{+0.14}_{-0.21}$	5.39	.71	.08	64.81	1.80	.06
+0.018	5.28	0.57	$^{+0.19}_{-0.32}$	4.04	.57	±0.09	47.49	1.66	±0.09
+0.035	8.87	0.87	$^{+0.11}_{-0.16}$	5.53	0.72	$^{+0.31}_{-1.66}$	136.64	2.13	$^{+0.19}_{-0.38}$

[a] All velocities are in km s^{-1} and distances in parsecs.

© American Astronomical Society • Provided by the NASA Astrophysics Data System

1987ApJ...317..676O

dispersion-size relation is largely determined by the accuracy of these corrections. Since we only have one set of data for determining the instrumental dispersion in each velocity system, we are not able to estimate the accuracy of our dispersion correction. The error bars in Figures 3 and 4 assume an uncertainty of 20%.

The results of these determinations of the dispersion are given in Table 5 and shown in Figure 3.

We also calculated the more analytically critical quantity, the structure function. For this application, the structure function (B) was calculated from

$$B = \langle | V(r') - V(r'') |^2 \rangle ,$$

where r' and r'' correspond to the positions of two points on the face of the nebula (Roy and Joncas 1985). The structure function was calculated for all combinations of points falling within the sample size. This function was also corrected for the instrumental dispersion. The results of this calculation are given in Table 6 and shown in Figure 4.

Like the dispersion, the structure function is also a measure of the dispersion of radial velocities, but has the powerful attraction that it directly uses all possible combinations of data. As such, it is inherently more sensitive to the exact nature of the turbulent process. The hook at the large-size end of the three nebulae studied over the entire face may be due to edge effects, as argued by Jean René Roy and his colleagues when this was encountered in M17 and S142; however, we believe it to be a mathematical selection effect when operating with the very small sample of data at the largest sample separations. This interpretation is supported by the very great uncertainties in the structure function at the largest separations and the fact that the same effect appears in the NGC 6514 and NGC 6523 data, which are sampled over only a small fraction of the nebular face. A study made by Castañeda (1985) with his very complete set of M42 data show that a hook appears only at the greatest separation when the sample size is small.

III. DISCUSSION

The data presented here constitute a unique body of material for testing models for turbulence in H II regions. The accompanying paper presents the predictions of the best models and compares these data, along with other observations that cover the entire face of a few nebulae, with the predictions in order to draw conclusions about the nature of the turbulence in H II regions. The reader is encouraged to study that work and a similar interpretation of NGC 1976 data (Castañeda and O'Dell 1987).

It is a pleasure to acknowledge the assistance and support of many individuals and institutions. Daryl Willmarth and the other Kitt Peak National Observatory staff members were stretched to the limit in helping the coudé feed system limp along until the necessary overhaul could be done. Here at Rice University David Golimowski performed much of the preparatory work on the data. Dr. John Jeff Hester, now of Cal Tech, developed the curve-fitting program and introduced the authors to the intricacies of the system. Our colleagues Jean René Roy and Gilles Joncas of the Université Laval have been generous with their ideas, preprints, and time.

Thanks are due to our underwriter, the National Aeronautics and Space Administration, through grants NAGW-384 and NAS5-29451 to the Rice University.

REFERENCES

Buscomb, W. 1963, Mount Stromlo Mineographs, No. 7.
Castañeda, H. O. 1985, *Bull. AAS*, **17**, 891.
Castañeda, H. O., and O'Dell, C. R. 1987, *Ap. J. (Letters)*, **315**, L55.
Elliot, K. H., Goudis, C., Hippelein, H., and Meaburn, J. 1984, *Astr. Ap.*, **138**, 451.
Fountain, W. F., Gary, G. A., and O'Dell, C. R. 1979, *Ap. J.*, **229**, 271.
———. 1983*a*, *Ap. J.*, **269**, 164.
———. 1983*b*, *Ap. J.*, **273**, 639.
Jensen, E. B., Talbot, R. J., Jr., and Dufour, R. J. 1981, *Ap. J.*, **243**, 716.
Lang, K. R. 1980, *Astrophysical Formulae* (Berlin: Springer Verlag), pp. 204 and 227.
Lynds, B. T., Canzian, B. J., and O'Neil, E. J., Jr. 1985, *Ap. J.*, **288**, 164.
Lynds, B. T., and O'Neil, E. J., Jr. 1982, *Ap. J.*, **263**, 130.
Mufson, S. L., Fountain, W. F., Gary, G. A., Howard, W. E., O'Dell, C. R., and Wolff, M. T. 1981, *Ap. J.*, **248**, 992.
Münch, G. 1958, *Rev. Mod. Phys.*, **30**, 1035.
O'Dell, C. R. 1986, *Ap. J.*, **304**, 767.
O'Dell, C. R., and Ball, M. E. 1985, *Ap. J.*, **289**, 526.
Roy, J. R., Arsenault, R., and Joncas, G. 1986, *Ap. J.*, **300**, 624.
Roy, J. R., and Joncas, G. 1985, *Ap. J.*, **288**, 142.
Scalo, J. M. 1984, *Ap. J.*, **277**, 556.
Wilson, O. C., Münch, G., Flather, E. M., and Coffeen, M. F. 1959, *Ap. J. Suppl.*, **4**, 199.
Woodard, C. E., Pipher, J. L., Helfer, H. L., Sharpless, S., Moneti, A., Kozikowski, D., Oliver, M., and Herter, T. 1986, *A.J.*, **91**, 870.

HECTOR O. CASTAÑEDA, C. R. O'DELL, and L. K. TOWNSLEY: Department of Space Physics and Astronomy, Rice University, P.O. Box 1892, Houston, TX 77251

© American Astronomical Society • Provided by the NASA Astrophysics Data System